Solid-State Electronics 201 (2023) 108583

Contents lists available at ScienceDirect

Solid State Electronics

journal homepage: www.elsevier.com/locate/sse

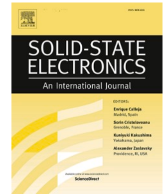

Surface scattering impact on Si/$TiSi_2$ contact resistance

Kantawong Vuttivorakulchai *, Mohammad Ali Pourghaderi, Gwang-Jun Kim, Seunghyun Song, Yoon-Suk Kim, Uihui Kwon, Dae Sin Kim

Computational Science and Engineering Team, Innovation Center, Device Solution Business, Samsung Electronics Co., Ltd., Hwaseong-si, Gyeonggi-do, Republic of Korea

ARTICLE INFO

The review of this paper was arranged by "Francisco Gamiz"

Keywords:
Contact resistance
Transmission
Surface scattering
Valley filtering
DFT-NEGF

ABSTRACT

This study reports the practical limit on contact resistance of Si (1 0 0)/$TiSi_2$ system. The maximum transmission in silicide contact is estimated via the overlap of conducting modes. This ideal limit is then compared versus the coherent transport calculation, where DFT-NEGF is applied to a pool of model interfaces. It is shown that interface scattering increases the contact resistance by an order of magnitude. The barrier tunneling strongly depends on surface termination and coordination defects. For the studied samples, the trend of contact resistance matches the inverse of transmission at Fermi level.

1. Introduction

The scaling of transistors in advanced nodes has effectively decreased the channel resistance. This makes the parasitic contributions particularly important, as they do not scale easily. Perhaps the most challenging component is the contact resistance. Currently, titanium silicide ($TiSi_2$) is the common choice of metal. In this study, some basic aspects of carrier transport in Si/$TiSi_2$ system are explored.

2. Theory and calculations

The samples of Si/C49-$TiSi_2$ junctions are prepared in (1 0 0) orientation. For this orientation, $TiSi_2$ may have five different terminations: Three Si-rich and two Ti-rich atomic planes. Fig. 1 shows the corresponding hetero-interfaces for all $TiSi_2$ terminations. The interface strain is about ~1 % of 1×1 nm^2 cross section with ~6 nm thickness of Si and $TiSi_2$.

2.1. Structure relaxation

The density functional theory (DFT) relaxation is performed using PseudoDojo pseudopotentials [1] with PBEsol functional and double-zeta polarized basis. The density cut-off energy is set to 150 Ha. The $\boldsymbol{k}$-grids of $3 \times 3 \times 1$ are applied for the density calculations. The atomic force for all samples is smaller than 20 meV/Å.

2.2. Contact resistance calculations

The contact resistance is calculated in two different ways: Valley filtering and DFT non-equilibrium Green's function (DFT-NEGF) methods. In the following, the results and details of each method are discussed.

- *Valley filtering limit*

Our procedure is similar to the work in Refs. [2] and [3]. After structural relaxation, the unit cells of bulk-representative parts are used for band structure calculations with uniform $\boldsymbol{k}$-grids of $101 \times 101 \times 101$. Here, band energies for both spin up and down are considered. meta-Generalized-Gradient Approximation (*meta*-GGA) exchange–correlation (XC) functional of Tran & Blaha (TB09) is used [4]. The c-parameter is set to 1.03511. The density mesh cut-off is at 100 Ha. The $\boldsymbol{k}$-resolved distribution of modes M (E, $\boldsymbol{k}$), which can be efficiently calculated using the so-called "band-counting" method, is then extracted for the relevant energy range. M (E) of Si and $TiSi_2$ are obtained by the integration over the 1st Brillouin zone. The valley filtering approach calculates the overlap between the $\boldsymbol{k}$-resolved distribution of modes in Si and $TiSi_2$. From the valley filtered M (E, $\boldsymbol{k}$), the contact resistance (ρ) is computed according to Landauer formalism [3]:

* Corresponding author.
E-mail address: k.vuttivorak@samsung.com (K. Vuttivorakulchai).

https://doi.org/10.1016/j.sse.2022.108583

Available online 30 December 2022
0038-1101/© 2022 Elsevier Ltd. All rights reserved.

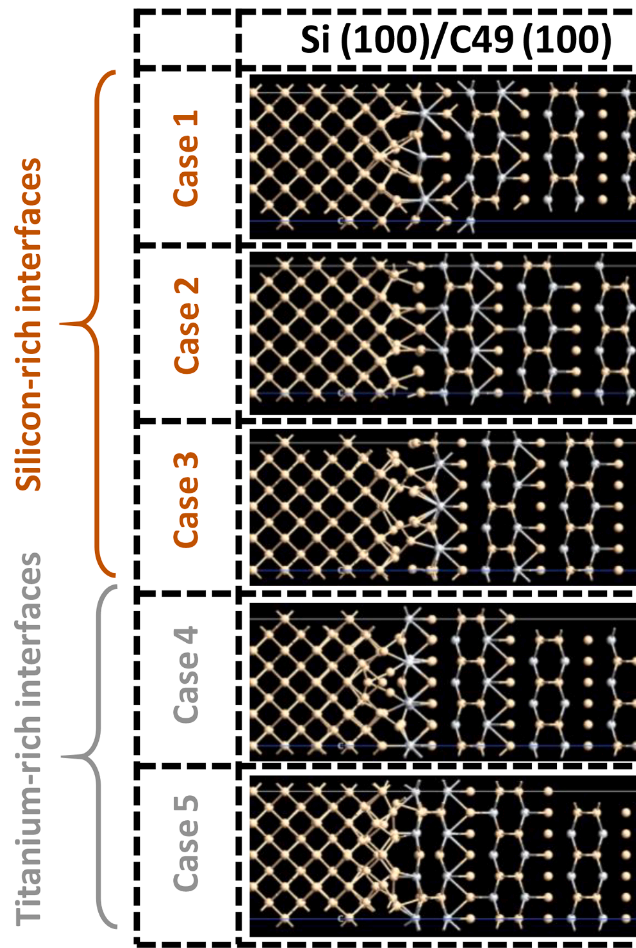

Fig. 1. The atomic structures of Si (1 0 0)/$TiSi_2$ (1 0 0) interfaces are shown after geometrical relaxation. Case 1–3 represent the Si-rich terminations, while case 4–5 are Ti-rich ones.

$$\frac{1}{\rho} = 2\cdot G_0 \int_{-\infty}^{\infty} M(E)\left(-\frac{\partial f}{\partial E}\right) dE, \quad (1)$$

where f is the Fermi-Dirac distribution function, $G_0 = 2q^2/\hbar$ is the fundamental quantum conductance, and q is the elementary charge. Fig. 2 shows the $\boldsymbol{k}$-resolved conducting modes of C49-$TiSi_2$, Si and the corresponding overlap. The conducting modes are effectively filtered in high energy range, as shown in Fig. 3(a). Consequently, the difference of intrinsic and valley-filtered resistance is increased at high carrier concentration, as shown in Fig. 3(b) and 3(c). Though these results consider the non-ideality of metal and mismatch of symmetries, the reflection and tunneling resistances at the interface are neglected. Therefore, these results can set the lowest theoretical limit for contact resistance.

- *DFT-NEGF calculations*

To investigate the impact of interface scattering, DFT-NEGF simulations are carried out. The basis and exchange–correlation setup is the same as mentioned previously. For all devices, silicon is n-type doped to 3×10^{20} cm^{-3} level [5], and transmission spectra are computed with regular $\boldsymbol{k}$-point grids of $51 \times 51 \times 1$. The resulting transmission per unit area, T (E), is used for the contact resistance calculation, as proposed in Ref. [6]. The typical $\boldsymbol{k}$-resolved transmissions are shown in Fig. 4. The transmissions across the hetero-interface are much lower than the ideal limit in Fig. 2. In particular, the conducting path near Γ-point is totally vanished for all cases. This is mainly due to the heavy effective mass in the longitudinal direction. To obtain an accurate density matrix, the $\boldsymbol{k}$-mesh should cover the detailed features of the silicon conduction band and metal Fermi surface. In Fig. 5(a), the sensitivity of contact resistance to the corresponding density matrix $\boldsymbol{k}$-mesh is demonstrated. The results are benchmarked against the reference case, where transmission mesh is 101×101, and density matrix mesh is 51×51. From these results, it can be seen that 13×13 $\boldsymbol{k}$-mesh keeps the error less than 1 %.

Fig. 5(b) shows the comparison of T (E) among five different interfaces. Apparently, the contact resistances in Fig. 5(c) are much larger than the theoretical limit, i.e. 5.9×10^{-11} $\Omega\cdot cm^2$. Interestingly, the atomic structure in case 3 gives the highest resistance. This is due to the fact that the specific Si-termination does not produce coordinate defects. As a result, the tunneling path between Si and the first metallic-plane gets longer, which effectively hampers the tunneling and transmission, as shown in Fig. 6. In general, the combination of bond-intimacy and coordination defects will determine the level of tunneling. The effective contribution of these factors can be presented by transmission at Fermi level, $T(E_f)$. As shown in Fig. 5(d), there is a strong correlation between contact resistance and $1/T(E_f)$. This suggests that $T(E_f)$ can be used as a metric for fast screening of model interfaces. Due to the form of the Fermi-Dirac distribution function, this metric becomes more exact as temperature is reduced.

3. Conclusions

The impact of interface chemistry on tunneling current in silicide contact is investigated. Among the prepared samples with similar Schottky barrier heights, those with shorter tunneling paths and

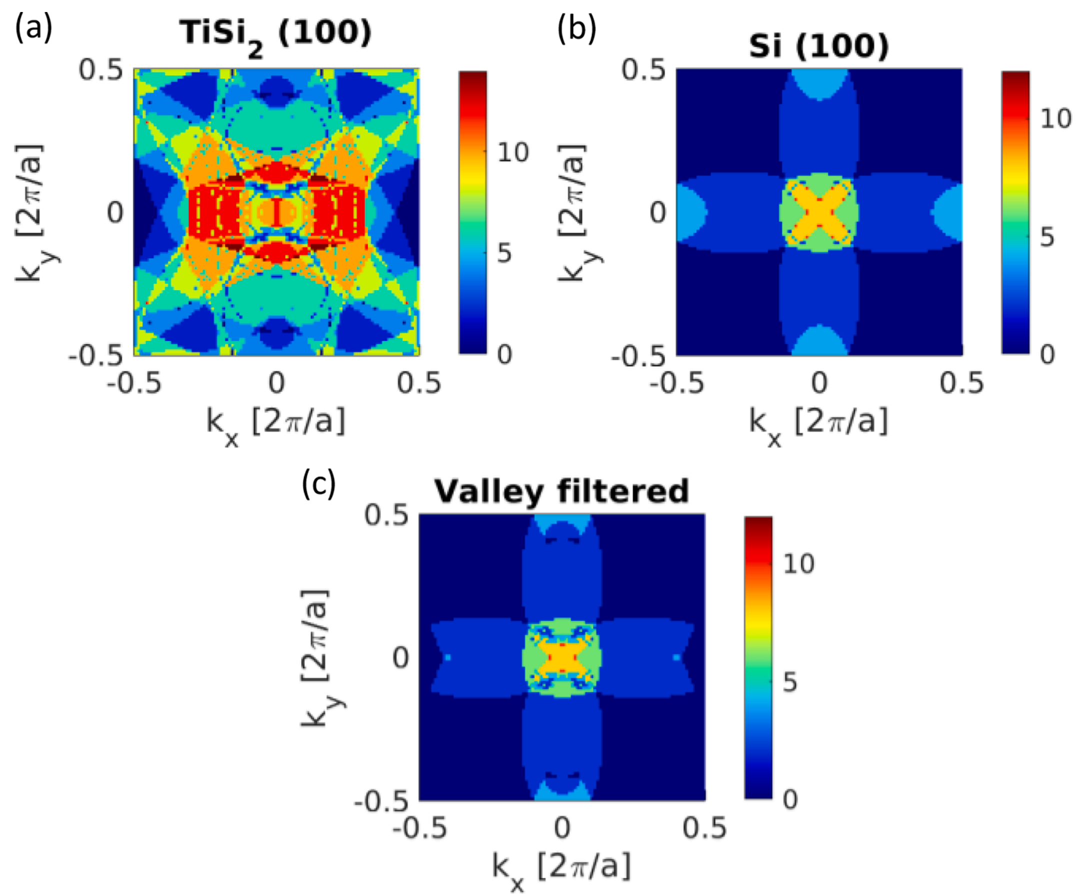

Fig. 2. (a) The transverse momentum-resolved distribution of modes (DOM) of $TiSi_2$. (b) Si with surface orientation in (1 0 0) direction. (c) Its valley filtered DOM. For these graphs, the energy level is at 0.134 eV from the conduction band minimum.

Solid State Electronics 201 (2023) 108583

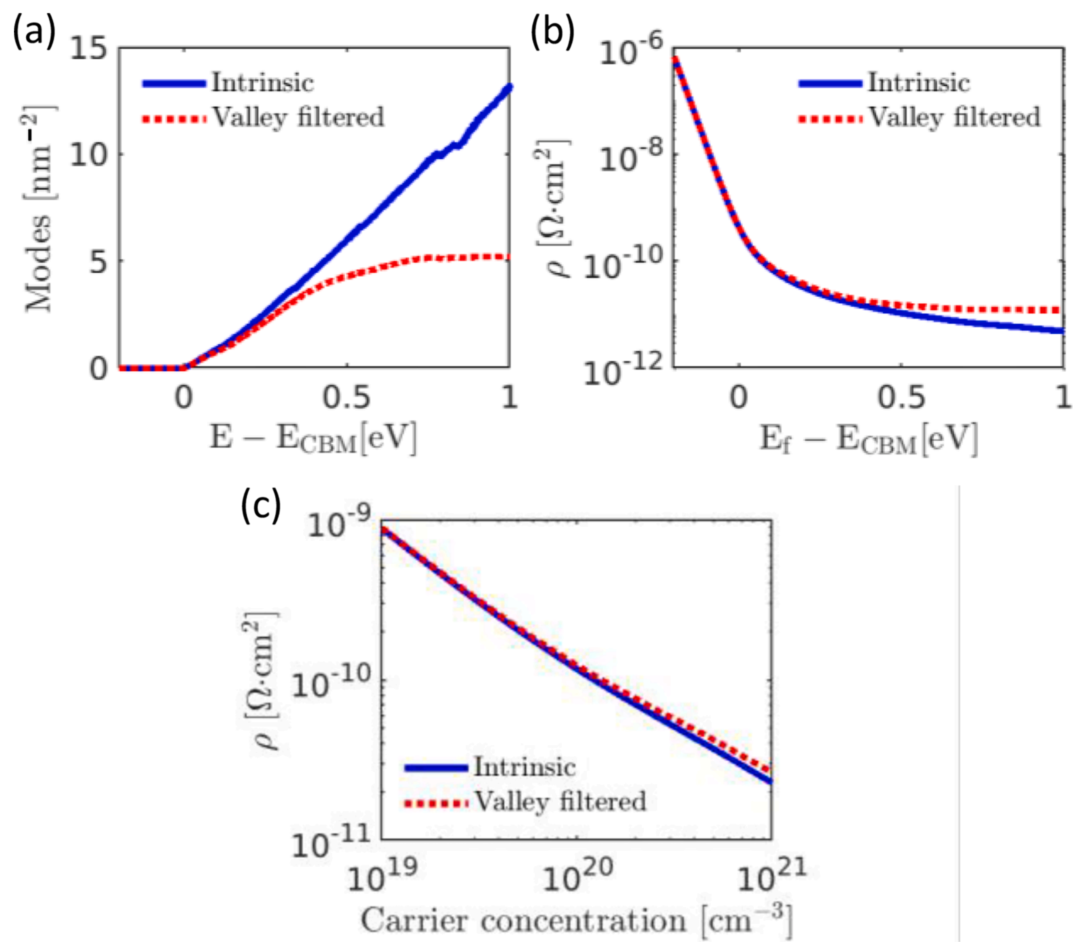

Fig. 3. The comparison between the intrinsic limit of Si and its valley filtered limit by $TiSi_2$ is shown at 300 K. (a) The available conducting modes per unit area, $M(E)$, are depicted versus energy. The reference energy is the conduction band minimum (CBM). (b) The resistances at different positions of Fermi level are shown, which represents the different doping scenarios. (c) The resistances as function of electron concentration are presented.

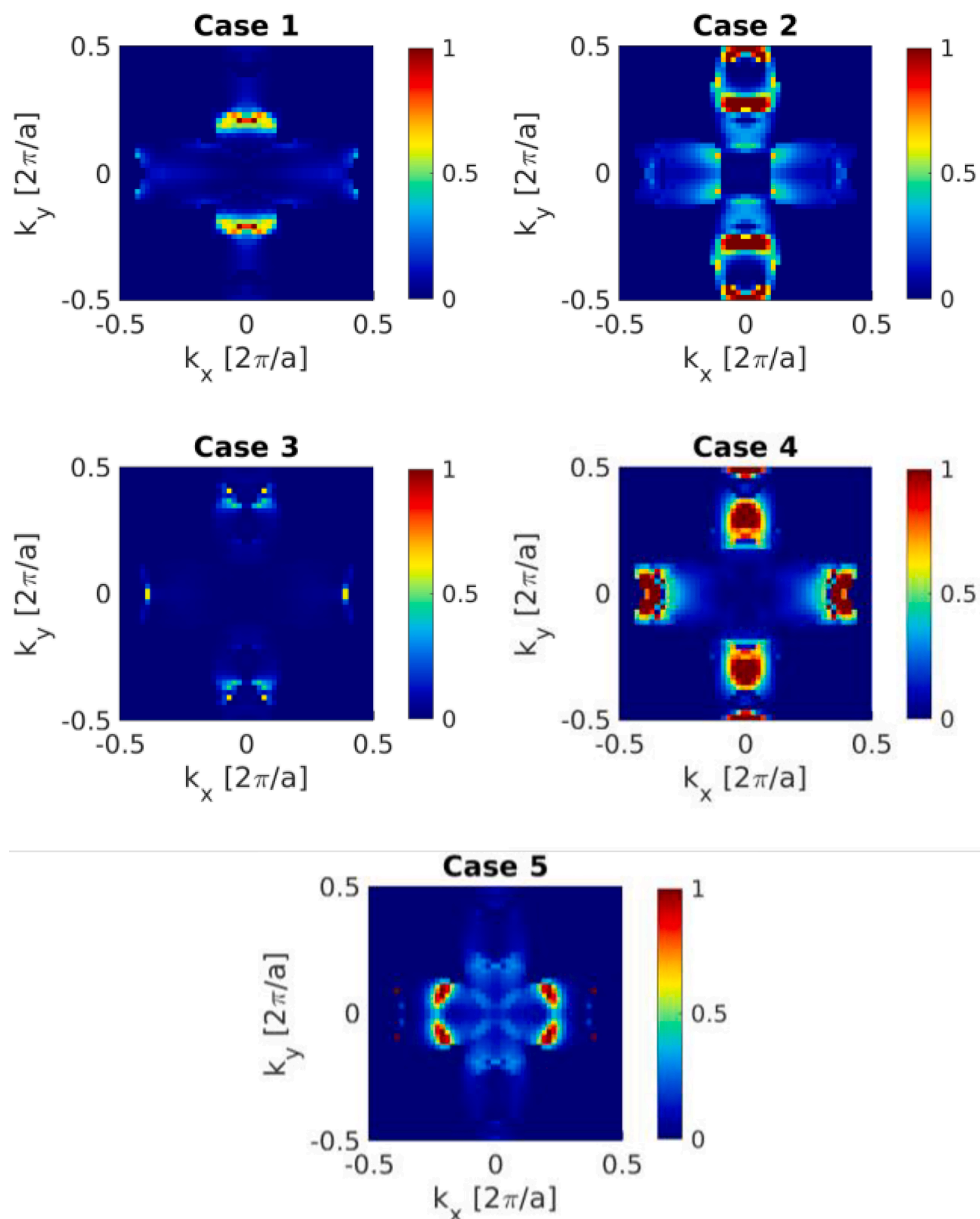

Fig. 4. The DFT-NEGF calculations of the transverse ***k***-resolved transmission spectra of Si (1 0 0)/$TiSi_2$ (1 0 0) model interfaces shown in Fig. 1. The results are demonstrated at Fermi level.

coordination defects closer to Fermi level produce lower contact resistance. For the nominal doping level, the tunneling current is much lower than the theoretical limit. This suggests that there is a big room to engineer the interface and optimize the contact resistance.

Declaration of Competing Interest

The authors declare the following financial interests/personal relationships which may be considered as potential competing interests: KANTAWONG VUTTIVORAKULCHAI reports financial support was provided by Samsung Electronics Co., Ltd.

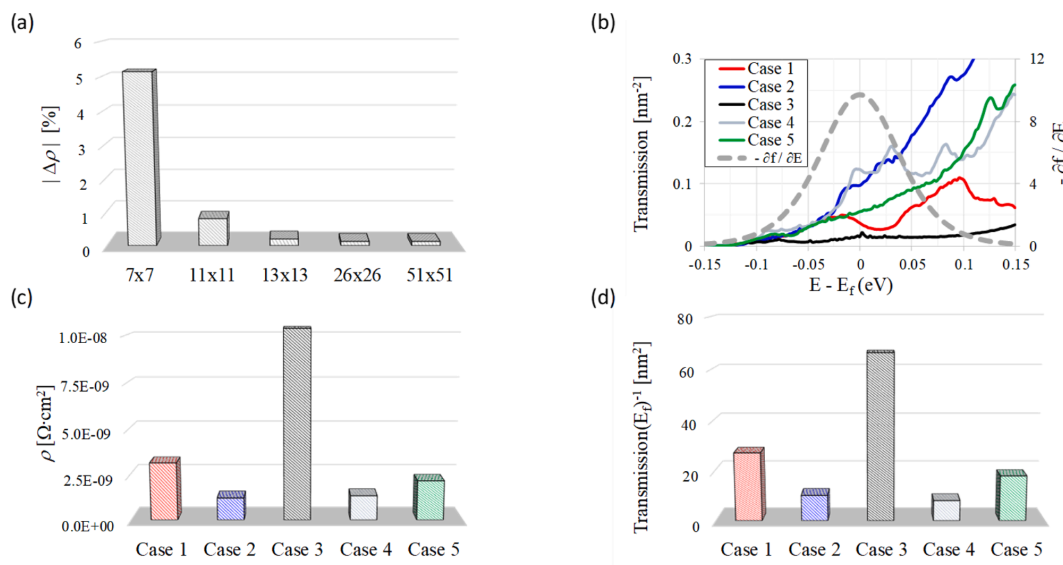

Fig. 5. (a) The sensitivity of contact resistance to density matrix ***k***-mesh resolution is shown for the structure of case 3. With 13x13 ***k***-mesh, the error is less than 1 %. (b) The transmissions per unit area of the 5 cases in Fig. 1 are benchmarked. (c) The corresponding resistances at room temperature are calculated. (d) The trend of inverse transmission at Fermi level of these 5 cases is shown.

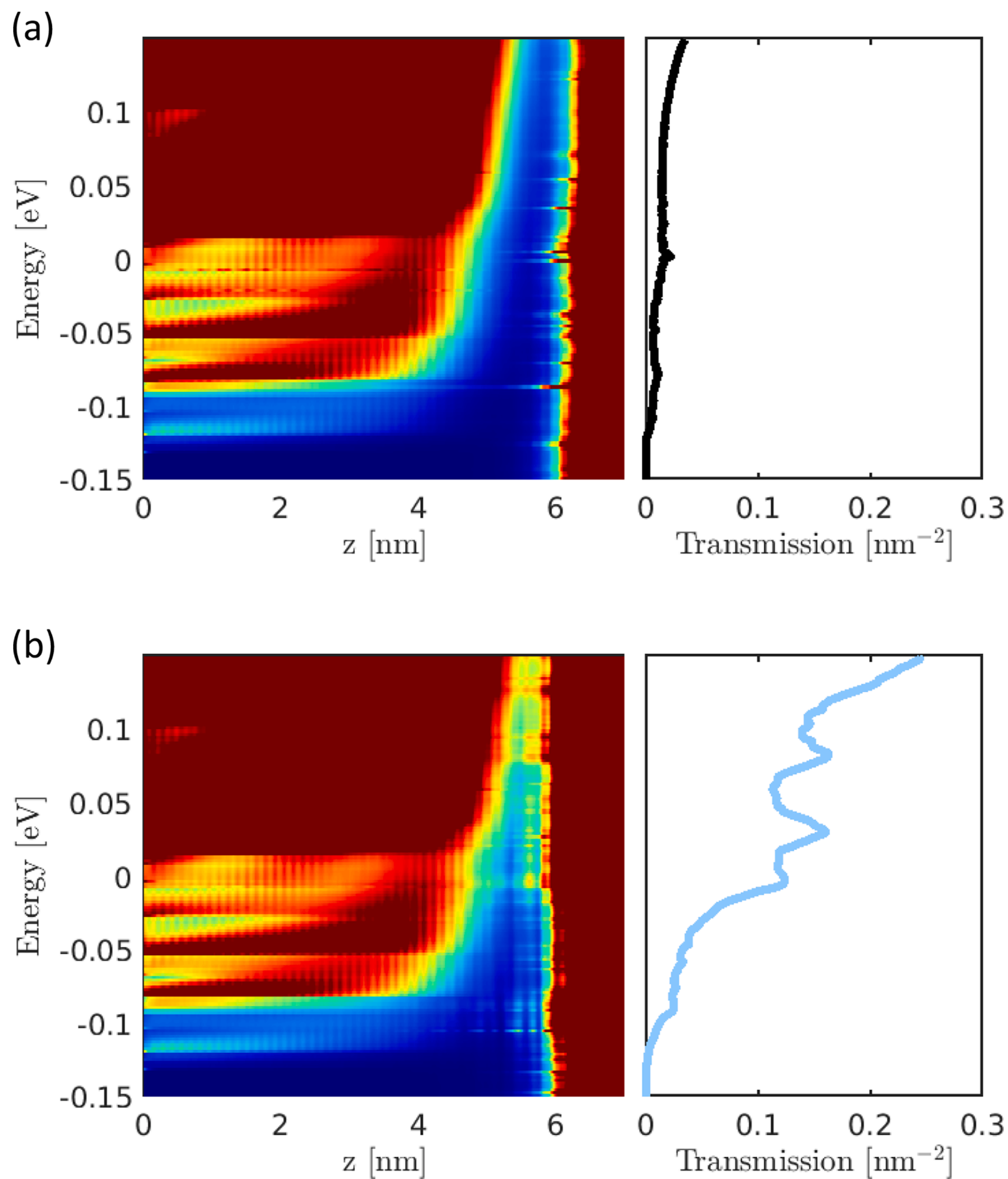

Fig. 6. The projected local density of states and the corresponding transmission from the structures of (a) case 3 and (b) case 4 are demonstrated.

Data availability

No data was used for the research described in the article.

References

[1] van Setten MJ, Giantomassi M, Bousquet E, Verstraete MJ, Hamann DR, Gonze X, et al. The PseudoDojo: Training and Grading a 85 Element Optimized Norm-conserving Pseudopotential Table. Comput Phys Commun 2018;226:39–54. https://doi.org/10.1016/j.cpc.2018.01.012.

[2] Hegde G, Bowen RC. Effect of Realistic Metal Electronic Structure on the Lower Limit of Contact Resistivity of Epitaxial Metal-Semiconductor Contacts. Appl Phys Lett 2014;105:053511. https://doi.org/10.1063/1.4892559.

[3] Maassen J, et al. Full Band Calculations of the Intrinsic Lower Limit of Contact Resistivity. Appl Phys Lett 2013;102:111605. https://doi.org/10.1063/1.4798238.

[4] Smidstrup S, et al. QuantumATK: An Integrated Platform of Electronic and Atomic-scale Modelling Tools. J Phys: Condens Matter 2019;32:015901. https://doi.org/10.1088/1361-648X/ab4007.

[5] Yu H, et al. Titanium Silicide on Si: P with Precontact Amorphization Implantation Treatment: Contact Resistivity Approaching 1×10^{-9} Ohm-cm2. IEEE Trans Electron Devices 2016;63:4632–41. https://doi.org/10.1109/TED.2016.2616587.

[6] Markussen T, Stokbro K. Metal-InGaAs Contact Resistance Calculations from First Principles. In: 2016 International Conference on Simulation of Semiconductor Processes and Devices (SISPAD); 2016. p. 373–6. https://doi.org/10.1109/SISPAD.2016.7605224.